

# Analytical and Numerical Bending Solutions for Thermoelastic Functionally Graded Rotating Disks with Non-uniform Thickness Based on Mindlin's Theory

A. Hassani\*, M. Gholami

Mechanical Engineering Department, Babol Noshirvani University of Technology, Babol, Iran.

## Article info

### Article history:

Received 18 March 2017

Received in revised form

19 August 2017

Accepted 15 September 2017

### Keywords:

Uniform thickness functionally graded rotating disk

Thermoelastic bending loading

Homotopy analysis method

Adomian's decomposition method

## Abstract

In this paper, analytical and numerical solutions for thermoelastic functionally graded (FG) rotating disks with non-uniform thickness under lateral pressure are studied. The study is performed based on Mindlin's theory. Considering the fact that bending and thermal loadings in analysis of rotating disk are necessary to study the components such as brake and clutch disks. The governing differential equations arising from FG rotating disk are firstly extracted. Then, Liao's homotopy analysis method (HAM) and Adomian's decomposition method (ADM) are applied as two analytical approaches. Calculation of stress components and then comparison of the results of HAM and ADM with Runge-Kutta's and FEM are performed to survey compatibility of their results. The distributions of radial and circumferential stresses of rotating disks are studied and discussed. Finally, the effects of temperature, grading index, angular velocity and lateral loading on the components of displacement and stresses are presented and discussed, in detail.

## Nomenclature

$a$	Inner radius	$A$	Integral constants
$b$	Outer radius	$B$	Integral constants
$E$	Young's modulus	$h(r)$	Thickness profile
$H_i$	Auxiliary functions	$\hbar_i$	Auxiliary parameters
$K$	Correction factor	$L_i$	Linear operators
$M_r, M_\theta$	Radial and hoop stress couples per unit length	$N_r, N_\theta$	Radial and hoop stress resultants per unit length
$N_i$	Nonlinear operators	$n_T$	Exponent in thermal distribution
$n_E$	Grading index in Young modulus distribution	$n_{qz}$	Exponent in transverse loading distribution
$n_\alpha$	Grading index in thermal expansion coefficient distribution	$n_\rho$	Grading index in mass density distribution
$q$	Embedding parameter	$Q_r$	Transverse shear resultant per unit length
$q_z$	Transverse loading	$T$	Temperature gradient
$U$	Total strain energy	$\Delta r$	Radial increment in Runge-Kutta method

\*Corresponding author: A. Hassani (Assistant Professor)

E-mail address: Hassani@nit.ac.ir

<http://dx.doi.org/10.22084/jrstan.2017.13316.1021>

ISSN: 2588-2597

$V$	Total external work	$Y_{i,m}$	Adomian's polynomials
$\alpha$	Thermal expansion coefficient	$\nu$	Poisson's ratio
$u_0$	In-plane radial displacement of the mid-plane	$u_r, u_z = w$	Radial and vertical displacements
$\varepsilon_r, \varepsilon_\theta, \gamma_{rz}$	Radial, hoop and transverse shear strains	$\sigma_r, \sigma_\theta, \sigma_{rz}$	Radial, hoop and transverse shear stresses
$\Pi$	Total elastic potential energy	$\rho$	Mass density
$\varphi_i, i = 1, 2, 3$	Unknown functions in homotopy analysis method	$\phi$	Rotation of a transverse normal in the plane $\theta = \text{constant}$
$\psi$	General unknown function in Runge-Kutta's method	$w$	Angular velocity

## 1. Introduction

Rotating disks are used in many practical applications such as steam and gas turbines, brake disks, and clutches. Brake disk and clutch are examples of rotating disks where body force and thermal and bending loading are involved. In gas turbine rotors, it is the pressure difference across the rotors that causes bending. In clutches and brakes, the force responsible for maintaining contact between the plates causes bending. These examples emphasize on the role of bending in design of rotating disks [1]. Application of variable thickness rotating disks is expanding chiefly for the sake of the economic consideration and practical optimization of mechanical performance [2].

For analytical solutions of rotating disks of uniform thickness, a closed-form solution is available. However, there is no straightforward solution to non-uniform rotating disk of variable properties.

Eraslan and Orcan [2] introduced an acceptable theoretical solution for rotating disks of exponentially variable thickness and linear hardening material without considering bending loading. Kordkheili and Naghdabadi [3] and Bayat et al. [4] presented a semi-analytical thermoelastic solution for functionally graded rotating disks with no bending loading. In recent years, Hojjati and Jafari [5, 6, 7] studied the elastic and elastic-plastic analyses of non-uniform thickness and density rotating disk by the variational iteration, homotopy perturbation and Adomian's decomposition methods. It is worth mentioning that in [7], the bilinear material and Tresca's yield criterion were utilized. Hojjati and Hassani [8] used the variable material properties technique to analyze variable thickness and density rotating disks with no lateral pressure by applying Von-Mises's yield criterion. Hassani and Hojjati [9] used variational iteration, Adomian's decomposition and homotopy analysis methods to solve the thermo-elastic analysis of FG rotating disk with variable thickness. Then, Hassani et al. [10] applied homotopy analysis method to analyze the non-uniform functionally graded thermo-elasto-plastic rotating disk by the bilinear material model and Von-Mises' yield criterion. Hassani et al. [11] also applied the variable material properties technique, Runge-Kutta's and fi-

nite element methods to analyze non-uniform thickness and material properties of rotating disks under thermo-elasto-plastic loading by using Von-Mises's yield criterion.

An investigation of in-plane free vibration of non-uniform thickness annular elliptic and circular elastic plates for all classical boundary conditions have been presented [12]. It is worth mentioning that in above-mentioned references, any bending effect has excluded. In the other words, the existent literatures of bending analysis of rotating disk are few.

Bayat et al. [1] studied bending analysis of FGM rotating disk under only centrifugal loading (with no thermal loading) by using semi-theoretical method of division of the disk into the number of sub-domains in radial direction.

In the beginning of the 1980s, Adomian [13] proposed so-called Adomian's decomposition method (ADM) for solving non-linear differential equations, while Liao in 1992 employed homotopy analysis method (HAM) to solve non-linear differential equations [14].

In recent years, Hosseini Kordkheili and Livani [15] studied thermoelastic creep behavior of a functionally graded rotating disk with varying thickness whose material properties were dependent on the temperature. Bayat et al. [16] investigated the magneto-thermo-mechanical response of a functionally graded annular variable-thickness rotating disk. The effects of the magnetic field, grading index and geometric non-linearity on the mechanical and thermal stresses of the annular disk were investigated. Ting and Hong-Liang [17] have been performed a thermo-elastic analysis of a functionally graded rotating annular disk with variable thickness rotating with an angular acceleration under a changing temperature field. The material properties were assumed to vary along the radial coordinate and related to the volume fraction of each material. The modulus of elasticity and the coefficient of thermal expansion were supposed to be temperature-dependent, while the Poisson's ratio was assumed to be constant. Also, Ting and Hong-Liang [17] presented an investigation on a rotating functionally graded piezoelectric material FGPM circular disk rotating around its axis at a constant angular velocity under a coupled hy-

grothermal field by finite difference method [18]. The material properties were assumed to vary along the radial coordinate exponentially. An analysis of a rotating functionally graded magneto-electro-elastic (FGMEE) circular disk with variable thickness under thermal environment was done [19]. The material was a mixture of piezoelectric (PE) and piezomagnetic (PM) materials, and the material properties were assumed to vary along the radius of the disk exponentially.

In this research, bending analysis of non-uniform thickness and material properties rotating disk under thermo-elastic loading based on first order shear deformation theory (Mindlin's theory) is studied. This study is undeniably required to comprehend how to treat the components such as brake disk and clutch. Firstly, the governing differential equations of FGM rotating disk on displacement field are extracted. Two analytical methods, namely HAM and ADM, are then considered for solving these equations. Then, the well-known Runge-Kutta's (RK) and finite element method are performed to compare with suggested methods. It is shown that there are good agreements between the results of four methods.

## 2. Deriving Equations of Rotating Disk

Consider a moderately thick axisymmetric FG disk. The disk rotates at the constant angular velocity  $w$  and is subjected to an axisymmetric transverse loading  $q_z(r)$  under temperature gradient.

Table (1) presents the characterization parameters defining the thickness profile  $h(r)$  and material properties to functionally graded rotating disk. In the following equation, the indices  $i$  and  $o$  in  $P$ , as a global property, indicate the values of respective parameters at the inner radius  $a$  and outer radius  $b$ . It is worth mentioning that in the present paper,  $E, \alpha, \rho, T$ , and  $q_z$  indicate Young's modulus, thermal expansion coefficient, mass density, temperature, and lateral pressure respectively. Furthermore, according to many practical specimens, the inner radius of the disk is clamped and the outer surface is free of any loading.

$$h(r) = h_0 \left( \frac{r}{b} \right)^{-n_h} \quad (1)$$

$$P(r) = (P_0 - P_i) \left( \frac{r-a}{b-a} \right)^{np} + P_i \quad (2)$$

**Table 1**

Characteristic parameters for the geometry, material properties and thermal loading.

Model	$a(m)$	$b(m)$	$h(m)$	$w(rad/s)$	$\nu$	$T(^{\circ}C)$	$\rho(Kg/m^3)$	$\alpha(1/^{\circ}C)$	$q_z(MPa)$	$E(GPa)$
D	0.2	0.5	$h_0 = 0.05$	500	0.3	$T_i = 150$	$\rho_i = 2700$	$\alpha_i = 23 \times 10^{-6}$	$q_{z,in} = 1$	$E_i = 70$
			$n_h = 0.3$			$T_o = 400$	$\rho_o = 5700$	$\alpha_o = 10 \times 10^{-6}$	$q_{z,out} = 1.4$	$E_o = 151$
						$n_T = 1$	$n_\rho = 1$	$n_\alpha = 1$	$n_{qz} = 1$	$n_E = 1$

The inner and outer surfaces of rotating disk are rich-metal and rich-ceramic, respectively [3].

### 2.1. Displacement Fields and Strains

The first-order shear deformation plate theory (FSDT) is the simplest one that accounts for non-zero transverse shear strain. It is based on the deformation fields as [20]:

$$u_r = u_r(r, z) = u_0(r) + z\varphi(r) \quad (3a)$$

$$u_z = u_z(r, z) = w(r) \quad (3b)$$

where  $u_0$  is the in-plane radial displacement of the mid-plane.  $u_r$  and  $u_z$  are the radial and vertical displacements respectively;  $\varphi = \varphi(r)$  denotes rotation of a transverse normal in the plane  $\theta = \text{constant}$ ;  $w = w(r)$  is the displacement along the thickness. Eqs. (3) yields constant values for the transverse shear strains and corresponding stress distributions. Since the real stress distribution in moderately thick plates is parabolic, this assumption is incorrect. Furthermore, it fails to satisfy the zero-stress condition on the top and bottom surfaces of the plate. Consequently, it was necessary to introduce a correction factor  $K$ , which was evaluated by comparison with the exact elastic solutions. Normally, the value of  $K$  is set equal to 5/6 [20].

The strain-displacement equations are calculated by the following [20]:

$$\varepsilon_r = \frac{\partial u_r}{\partial r} = \frac{du_0}{sdr} + z \frac{d\varphi}{dr} - \alpha T, \quad (4a)$$

$$\varepsilon_\theta = \frac{u_r}{r} = \frac{u_0}{r} + z \frac{\varphi}{r} - \alpha T, \quad (4b)$$

$$\gamma_{rz} = 2\varepsilon_{rz} = \frac{\partial u_r}{\partial z} + \frac{\partial u_z}{\partial r} = \varphi + \frac{dw}{dr}, \quad (4c)$$

in which,  $\varepsilon_r$  and  $\varepsilon_\theta$  are mechanical strains and not total strains. It can be noted that

$$\gamma_{r\theta} = \varepsilon_{r\theta} = 0, \quad \gamma_{\theta z} = \varepsilon_{\theta z} = 0, \quad \varepsilon_z = \frac{dw}{dz} = 0.$$

The constitutive equations are applied as the following [20]:

$$\begin{bmatrix} \sigma_r \\ \sigma_\theta \\ \sigma_{rz} \end{bmatrix} = \frac{E(r)}{1-\nu^2} \begin{bmatrix} 1 & \nu & 0 \\ \nu & 1 & 0 \\ 0 & 0 & \frac{1-\nu}{2} \end{bmatrix} \begin{bmatrix} \varepsilon_r \\ \varepsilon_\theta \\ \gamma_{rz} \end{bmatrix} \quad (5)$$

## 2.2. Equilibrium Equations

If  $U$  is the total strain energy and  $V$  is the total external work done on the body by the external forces, then the total elastic potential energy  $\Pi$  can be represented as:

$$\Pi = U - V \quad (6)$$

The theorem of minimum potential energy is defined as the following: Of all the displacements satisfying compatibility and the prescribed boundary conditions,

$$\delta \Pi = \delta(U - V) \quad (9)$$

$$= 2\pi \left\{ \int_{r_1}^{r_2} \left[ r \times \left( N_r \frac{d\delta u_0}{dr} + M_r \frac{d\delta\varphi}{dr} + Q_r \left( \delta\varphi + \frac{d\delta w}{dr} \right) + N_\theta \frac{\delta u_0}{r} + M_\theta \frac{\delta\varphi}{r} \right) - r(q_z \delta w + \rho r w^2 h \delta u_0) \right] \times dr \right\} = 0$$

where,

$$(N_r, N_\theta, Q_r) = \int_{-\frac{h}{2}}^{\frac{h}{2}} (\sigma_r, \sigma_\theta, \sigma_{rz}) dz, \quad (10)$$

$$(M_r, M_\theta) = \int_{-\frac{h}{2}}^{\frac{h}{2}} (\sigma_r, \sigma_\theta) z dz \quad (11)$$

$N_r = N_r(r)$ ,  $N_\theta = N_\theta(r)$  are the stress resultants per unit length,  $M_r = M_r(r)$ ,  $M_\theta = M_\theta(r)$  are the stress couples per unit length,  $Q_r = Q_r(r)$  is the transverse shear resultant per unit length. The well-known Euler-Lagrange equations are used for Eq. (9) and it will result in three following differential equations:

$$\delta u_0 : N_\theta - \rho r^2 w^2 h - N_r - r \frac{dN_r}{dr} = 0 \quad (12a)$$

$$\delta\varphi : M_\theta + rQ_r - M_r - r \frac{dM_r}{dr} = 0 \quad (12b)$$

$$\delta w : q_z r + Q_r + r \frac{dQ_r}{dr} = 0 \quad (12c)$$

And the following boundary conditions are obtained from  $\delta u_0$ ,  $\delta\varphi$ , and  $\delta w$ , respectively:

$$u_r = 0 \quad \text{OR} \quad N_r = 0 \quad (13a)$$

$$\varphi = 0 \quad \text{OR} \quad M_r = 0 \quad (13b)$$

$$w = 0 \quad \text{OR} \quad Q_r = 0 \quad (13c)$$

Substituting for  $\sigma_r$ ,  $\sigma_\theta$ , and  $\sigma_{rz}$  from Eq. (5) in to Eqs. (10) and (11), one has:

$$N_r(r) = \frac{Eh}{1-\nu^2} \left( \frac{du_0}{dr} - \alpha T \right) + \frac{Eh\nu}{1-\nu^2} \left( \frac{u_0}{r} - \alpha T \right) \quad (14a)$$

those that satisfy equilibrium equations make the potential energy a minimum [21,22].

The principle of minimum total potential energy expressed that  $\delta \Pi = \delta(U - V) = 0$ , in which [20-22]:

$$\delta U = \int \int_R \left[ \int_{-\frac{h}{2}}^{\frac{h}{2}} (\sigma_r \delta\epsilon_r + \sigma_{rz} \delta\gamma_{rz} + \sigma_\theta \delta\epsilon_\theta) dz \right] r dr d\theta \quad (7)$$

$$\delta V = \int \int_R (q_z \delta w + \rho r w^2 h \delta u_0) r dr d\theta \quad (8)$$

If note to have axisymmetric geometry and loading, Eqs. (7) and (8) are resulted in:

$$N_\theta(r) = \frac{Eh}{1-\nu^2} \left( \frac{u_0}{r} - \alpha T \right) + \frac{Eh\nu}{1-\nu^2} \left( \frac{du_0}{dr} - \alpha T \right) \quad (14b)$$

$$Q_r(r) = \frac{KEh}{2(1+\nu)} \left( \frac{dw}{dr} + \varphi \right) \quad (14c)$$

$$M_r(r) = \frac{Eh^3}{12(1-\nu^2)} \left( \frac{d\varphi}{dr} \right) + \frac{Eh^3\nu}{12(1-\nu^2)} \left( \frac{\varphi}{r} \right) \quad (14d)$$

$$M_\theta(r) = \frac{Eh^3}{12(1-\nu^2)} \left( \frac{\varphi}{r} \right) + \frac{Eh^3\nu}{12(1-\nu^2)} \left( \frac{d\varphi}{dr} \right) \quad (14e)$$

Substituting for various terms from Eqs. (14) in to Eqs. (12) yields a set of three ordinary differential equations for displacement fields as the following:

$$rE \frac{d^2 u_0}{dr^2} + \frac{1}{h} \frac{d}{dr} (rEh) \frac{du_0}{dr} + \frac{1}{h} \left( \nu \frac{d}{dr} (Eh) - \frac{Eh}{r} \right) u_0 - \frac{r(1+\nu)}{h} \frac{d}{dr} (Eh\alpha T) + (1-\nu^2)\rho r^2 w^2 = 0 \quad (15a)$$

$$rE \frac{d^2 \varphi}{dr^2} + \frac{1}{h} \left( rh \frac{dE}{dr} + 3rE \frac{dh}{dr} + Eh \right) \frac{d\varphi}{dr} - \frac{6rKE(1-\nu)}{h^2} \frac{dw}{dr} + \frac{1}{rh^2} \left( h^2 \frac{dE}{dr} r\nu + 3hE \frac{dh}{dr} r\nu - Eh^2 - 6r^2KE(1-\nu) \right) \varphi = 0 \quad (15b)$$

$$rE \frac{d^2 w}{dr^2} + \frac{1}{h} \frac{d}{dr} (rEh) \times \frac{dw}{dr} + rE \frac{d\varphi}{dr} + \frac{1}{h} \frac{d}{dr} (rEh) \times \varphi + \frac{2r(1+\nu)}{Kh} q_z = 0 \quad (15c)$$

It may be noted that Eqs. (15) are different from the one considered by Bayat et al. [1]. Unlike Ref. [1], thermal loading, variations of thickness and of thermal

expansion coefficient of the disk versus the radius have been considered herein.

Eq. (15a) is independent of two other Eqs. (15b) and (15c); However, Eqs. (15b) and (15c) are coupled which are difficult even to solve by well-known Runge-Kutta's method. In order to overcome this problem, the following strategy is continued:

Eq. (12c) is differentiated to derive  $Q_r(r)$ . This yields to the following equation:

$$Q_r(r) = \frac{-\int r q_z(r) dr + c_1}{r} \quad (16)$$

where  $c_1$  can be determined by identifying the boundary conditions of  $Q_r(r)$  at inner or outer radii of the disk.

By substituting Eq. (16) into Eq. (12b), one has:

$$M_\theta - \int r q_z(r) dr + c_1 - M_r - r \frac{dM_r}{dr} = 0 \quad (17)$$

By substituting Eqs. (14d) and (14e) into Eq. (17), one has the following equation:

$$\begin{aligned} rE \frac{d^2 \varphi}{dr^2} + \frac{\left( h^3 r^2 \frac{dE}{dr} + Eh^3 r + 3h^2 \frac{dh}{dr} Er^2 \right)}{rh^3} \frac{d\varphi}{dr} \\ - \frac{\left( -h^3 r \nu \frac{dE}{dr} - 3h^2 \frac{dh}{dr} Er \nu + Eh^3 \right)}{rh^3} \varphi \\ + \frac{12 \left( \int r q_z dr - c_1 \right) (1 - \nu^2)}{h^3} = 0 \end{aligned} \quad (18a)$$

By substituting Eq. (16) into Eq. (14c), one has:

$$\begin{aligned} rE \frac{dw}{dr} + rE\varphi + \frac{2}{Kh}(1 + \nu) \left( \int r q_z dr \right) \\ - \frac{2c_1}{Kh}(1 + \nu) = 0 \end{aligned} \quad (18b)$$

As it is seen, Eqs. (15a) and (18a) are uncoupled and are able to be individually solved. Eq. (18b) may be solved by using the solution of  $\varphi(r)$  to obtain  $w(r)$ .

In order to solve the mentioned differential equations by means of analytical methods, they are rewritten as the following:

$$\begin{aligned} \frac{d^2 u_0}{dr^2} + \frac{1}{rEh} \frac{d}{dr} (rEh) \frac{du_0}{dr} + \frac{1}{rEh} \left( \nu \frac{d}{dr} (Eh) - \frac{Eh}{r} \right) u_0 \\ - \frac{(1 + \nu)}{Eh} \frac{d}{dr} (Eh\alpha T) + \frac{(1 - \nu^2)\rho r w^2}{E} = 0 \end{aligned} \quad (19a)$$

$$\begin{aligned} \frac{d^2 \varphi}{dr^2} + \frac{1}{rh^3 E} \left( h^3 r \frac{dE}{dr} + Eh^3 + 3h^2 \frac{dh}{dr} Er \right) \frac{d\varphi}{dr} \\ - \frac{1}{r^2 h^3 E} \left( -h^3 r \nu \frac{dE}{dr} - 3h^2 \frac{dh}{dr} Er \nu + Eh^3 \right) \varphi \\ + \frac{12 \left( \int r q_z dr - c_1 \right) (1 - \nu^2)}{rEh^3} = 0 \end{aligned} \quad (19b)$$

$$\begin{aligned} \frac{dw}{dr} + \varphi + \frac{2}{rEKh}(1 + \nu) \left( \int r q_z dr \right) \\ - \frac{2c_1}{rEKh}(1 + \nu) = 0 \end{aligned} \quad (19c)$$

### 3. Solution of FG Rotating Disk

In this section, the procedure of solving FG rotating disk subjected to lateral pressure through HAM, ADM and Runge-Kutta's method is presented.

#### 3.1. Homotopy Analysis Method (HAM)

HAM is based on a continuous variation from an initial trial to the exact solution. A Maclaurin series expansion provides a successive approximation of solution through repeated application of a differential operator with initial trial as the first term [14]. Because of saving space, the background of HAM is not presented herein. In order to introduce HAM, the audiences are referred to Author's papers [9,10] and [14].

Herein, the elastic equations of annular rotating disks with variable thickness and material properties subjected to lateral loading, defined by Eqs. (19) are considered. To solve Eqs. (19) using HAM, the linear operators  $L_i$ ,  $i = 1, 2, 3$  corresponding to Eqs. (19a)-(19c), respectively, can be chosen as:

$$\begin{aligned} L_i[\phi_i(r; q)] &= \frac{d^2 \phi_i(r; q)}{dr^2}, \quad \text{For } i = 1, 2 \\ L_3[\phi_3(r; q)] &= \frac{d^2 \phi_3(r; q)}{dr} \end{aligned} \quad (20)$$

where  $q \in [0, 1]$  is the embedding parameter and  $\phi_i$ ,  $i = 1, 2, 3$  are unknown functions corresponding with  $u_0(r)$ ,  $\varphi(r)$ ,  $w(r)$  respectively.

The following initial approximations can be chosen:

$$\begin{aligned} u_{0,0}(r) &= A_{1,0} + B_{1,0}r \\ \varphi_0(r) &= A_{2,0} + B_{2,0}r \\ w_0(r) &= A_{3,0} \end{aligned} \quad (21)$$

in which  $A_{i,0}$  and  $B_{i,0}$  are determined using boundary conditions.

By attention to Eqs. (19) and HAM algorithm, one

can suggest the nonlinear operators as:

$$\begin{aligned}
 N_1[\phi_1(r; q)] &= \frac{d^2\phi_1(r; q)}{dr^2} + \frac{1}{rEh} \frac{d}{dr}(rEh) \frac{d\phi_1(r; q)}{dr} \\
 &+ \frac{1}{rEh} \left( \nu \frac{d}{dr}(Eh) - \frac{Eh}{r} \right) \phi_1(r; q) - \frac{(1+\nu)}{Eh} \frac{d}{dr}(Eh\alpha T) \\
 &+ \frac{(1-\nu^2)\rho rw^2}{E} \quad (22a)
 \end{aligned}$$

$$\begin{aligned}
 N_2[\phi_2(r; q)] &= \frac{d^2\phi_2(r; q)}{dr^2} \\
 &+ \frac{1}{rh^3E} \left( h^3r \frac{dE}{dr} + Eh^3 + 3h^2 \frac{dh}{dr} Er \right) \frac{d\phi_2(r; q)}{dr} \\
 &- \frac{1}{r^2h^3E} \left( -h^3r\nu \frac{dE}{dr} - 3h^2 \frac{dh}{dr} Er\nu + Eh^3 \right) \phi_2(r; q) \\
 &+ \frac{12 \left( \int rq_z dr - c_1 \right) (1-\nu^2)}{rEh^3} \quad (22b)
 \end{aligned}$$

$$\begin{aligned}
 N_3[\phi_2(r; q), \phi_3(r; q)] &= \frac{d\phi_3(r; q)}{dr} + \phi_2(r; q) \\
 &+ \frac{2}{rEKh} (1+\nu) \left( \int rq_z dr \right) - \frac{2c_1}{rEKh} (1+\nu) \quad (22c)
 \end{aligned}$$

where  $N_i, i = 1, 2, 3$  are nonlinear operators corresponding with Eqs. (19a) to (19c), respectively. In order to speed up the solution and reducing hardware requisitions and based on the so-called rule of solution existence [14], and Auxiliary functions  $H_i(r)$  are considered in the following form:

$$H_i(r) = \frac{1}{r}, \quad i = 1, 2, 3 \quad (23)$$

The index  $i$  corresponds to Eqs. (19a) to (19b), respectively. So, from here to end,  $H_i(r)$  denotes  $H(r) = 1/r$ . The  $m$ th-order deformation equations are written as:

$$u_{0,m}(r) = \mathcal{X}_m u_{0,m-1}(r) + \hbar_1 L_1^{-1} [H(r) R_{1,m}(u_{0,m-1})] \quad (24a)$$

$$\varphi_m(r) = \mathcal{X}_m \varphi_{m-1}(r) + \hbar_2 L_2^{-1} [H(r) R_{2,m}(\varphi_{m-1})] \quad (24b)$$

$$w_m(r) = \mathcal{X}_m w_{m-1}(r) + \hbar_2 L_3^{-1} [H(r) R_{3,m}(\varphi_{m-1}, w_{m-1})] \quad (24c)$$

Subject to the boundary conditions of:

$$\begin{aligned}
 u_{0,m}(a) = 0, \quad u_{0,m}(b) = 0 & \quad \text{for } m \geq 1 \\
 \varphi_m(a) = 0, \quad \varphi_m(b) = 0 & \quad \text{for } m \geq 1 \\
 w_m(a) = 0, & \quad \text{for } m \geq 1
 \end{aligned} \quad (25)$$

where  $\hbar_i, i = 1, 2$  are auxiliary parameters with no physical content and  $\mathcal{X}_m = \begin{cases} 1, & m = 1 \\ 0, & m \geq 2 \end{cases}$ .

From Eqs. (24), one can obtain the high-order approximation of the unknown functions  $u_0(r), \varphi(r)$  and  $w(r)$ . Herein, one has to calculate  $R_{i,m}(m \geq 1), i = 1, 2, 3$ .

$R_{i,m}(m \geq 1), i = 1, 2, 3$  for  $u_0(r), \varphi(r)$  and  $w(r)$ , respectively, are determined as the following:

$$\begin{aligned}
 R_{1,m}(u_{0,m-1}) &= \frac{d^2 u_{0,m-1}}{dr^2} + \frac{1}{rEh} \frac{d}{dr}(rEh) \frac{du_{0,m-1}}{dr} \\
 &+ \frac{1}{rEh} \left( \nu \frac{d}{dr}(Eh) - \frac{Eh}{r} \right) u_{0,m-1}(r) \\
 &+ \zeta_m \left[ -\frac{(1+\nu)}{Eh} \frac{d}{dr}(Eh\alpha T) + \frac{(1-\nu^2)\rho rw^2}{E} \right] \quad (26a)
 \end{aligned}$$

$$\begin{aligned}
 R_{2,m}(\varphi_{m-1}) &= \frac{d^2 \varphi_{m-1}}{dr^2} \\
 &+ \frac{1}{rh^3E} \left( h^3r \frac{dE}{dr} + Eh^3 + 3h^2 \frac{dh}{dr} Er \right) \frac{d\varphi_{m-1}}{dr} \\
 &- \frac{1}{r^2h^3E} \left( -h^3r\nu \frac{dE}{dr} - 3h^2 \frac{dh}{dr} Er\nu + Eh^3 \right) \varphi_{m-1} \\
 &+ \zeta_m \left[ \frac{12 \left( \int rq_z dr - c_1 \right) (1-\nu^2)}{rEh^3} \right] \quad (26b)
 \end{aligned}$$

$$\begin{aligned}
 R_{2,m}(\varphi_{m-1}) &= \frac{d^2 \varphi_{m-1}}{dr^2} \\
 &+ \frac{1}{rh^3E} \left( h^3r \frac{dE}{dr} + Eh^3 + 3h^2 \frac{dh}{dr} Er \right) \frac{d\varphi_{m-1}}{dr} \\
 &- \frac{1}{r^2h^3E} \left( -h^3r\nu \frac{dE}{dr} - 3h^2 \frac{dh}{dr} Er\nu + Eh^3 \right) \varphi_{m-1} \\
 &+ \zeta_m \frac{12}{rEh^3} \left( \int rq_z dr - c_1 \right) (1-\nu^2) \quad (26c)
 \end{aligned}$$

$$\text{in which, } \zeta_m = \begin{cases} 1, & m = 1 \\ 0, & m \geq 2 \end{cases}$$

By employing the selected linear operators  $L_i, i = 1, 2, 3$ , Eqs. (24) reduce to

$$\begin{aligned}
 u_{0,m}(r) &= \mathcal{X}_m u_{0,m-1}(r) \\
 &+ \hbar_1 \int \int (H(r) \times R_{1,m}) dr dr + A_{1,m} + B_{1,m} r \quad (26d)
 \end{aligned}$$

$$\begin{aligned}
 \varphi_m(r) &= \mathcal{X}_m \varphi_{m-1}(r) \\
 &+ \hbar_2 \int \int (H(r) \times R_{2,m}) dr dr + A_{2,m} + B_{2,m} r \quad (26e)
 \end{aligned}$$

$$w_m(r) = \mathcal{X}_m w_{m-1}(r) + \hbar_2 \int \int (H(r) \times R_{3,m}) dr dr + A_{3,m} \quad (26f)$$

where  $A_{1,m}, A_{2,m}, A_{3,m}, B_{1,m}$  and  $B_{2,m}$  are integral constants which are determined by boundary conditions of Eq. (25). It is worth mentioning that  $c_1$  is determined by boundary condition of  $Q_r$  at inner or outer radii of the disk.

Finally, the  $m$ th-order approximations of  $u_0, \varphi$  and  $w$  can be expressed, respectively, as:

$$\begin{aligned} u_0(r) &\approx \sum_{i=0}^{i=m} u_{0,i}(r) \\ \varphi(r) &\approx \sum_{i=0}^{i=m} \varphi_i(r) \\ w(r) &\approx \sum_{i=0}^{i=m} w_i(r) \end{aligned} \quad (27)$$

Eqs. (27) is a family of solution expressions in terms of auxiliary parameters. Coefficients, and are calculated by boundary conditions of the disk during the process of solution. Different kinds of boundary conditions for rotating disk, namely roller supported-free boundary conditions, hinged-free boundary conditions and clamped-free boundary conditions may be considered [23]. In this research, clamped-free boundary conditions are considered. For clamped-free boundary conditions, it can be expressed as [23]:

$$\begin{aligned} \text{At } r = a; \quad &u_0 = 0, \quad \varphi = 0, \quad w = 0 \\ \text{At } r = b; \quad &N_r = 0, \quad M_r = 0, \quad Q_r = 0 \end{aligned} \quad (28)$$

By employing the boundary conditions (28) and using Eqs. (27) for  $u_0, \varphi, w$  and Eqs. (14a), (14c) and (14d) for  $N_r, Q_r$  and  $M_r$ , respectively, one can easily determine the coefficients  $A_{1,0}, A_{2,0}, A_{3,0}, B_{1,0}, B_{2,0}$  and  $c_1$ . Herein,  $c_1$  is determined by boundary conditions of outer radius of the disk.

In order to show the influence of  $\hbar_i, i = 1, 2$  on the convergence of  $m$ th-order approximations (in Eqs. 27),  $u_0(r)$  and  $w(r)$  are first plotted versus  $\hbar_i, i = 1, 2$ , respectively. The curves  $u_0(r)$  versus  $\hbar_1$  and  $w(r)$  against  $\hbar_2$  contain a horizontal line segment over the valid regions. Liao called such kind of curve the  $\hbar$ -curve [14], which clearly indicates the valid region of a solution series. In general, by means of  $\hbar$ -curves, it is straight forward to find the corresponding valid region of  $\hbar$ . By choosing a value of  $\hbar$  in the valid region, it can be ensured that the corresponding solution series is convergent to exact solution. In this way, one can control and adjust the convergence region and rate of solution series. The  $\hbar$ -curve of  $u_0(r)$  and  $\varphi(r)$  at the

mid-radius of rotating disk for 10th-order approximation of them are shown in Fig. 1 and Fig. 2, respectively. From these figures, it is easy to discover that the valid region of  $\hbar_1$  for the given rotating disk is  $-0.45 \leq \hbar_1 \leq -0.2$  and by attention to Fig. 2, valid region of  $\hbar_2$  is  $-0.4 \leq \hbar_2 \leq -0.2$ . So, in this research, the value of  $\hbar_1$  and  $\hbar_2$  are respectively selected -0.3 and -0.27.

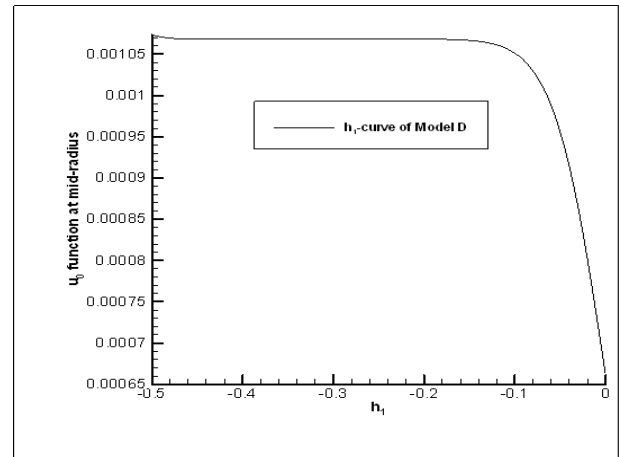


Fig. 1.  $\hbar_1$ -curve of 10th-order approximation of  $u_0(r)$  at middle radius of model D obtained by HAM.

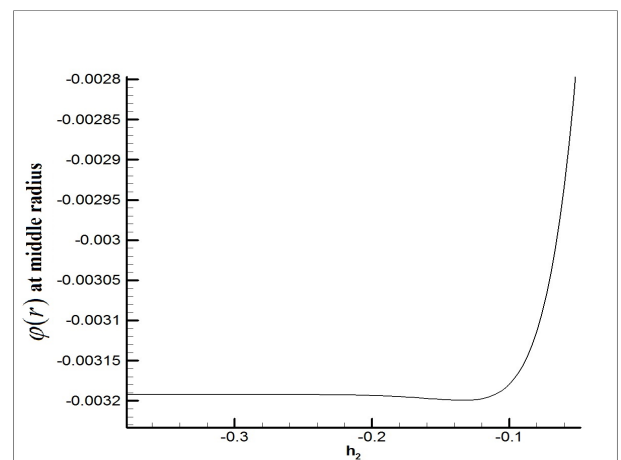


Fig. 2.  $\hbar_2$ -curve of 10th-order approximation of  $\varphi(r)$  at middle radius of model D obtained by HAM.

### 3.2. Adomian's Decomposition Method (ADM)

ADM approaches any equation, linear or nonlinear in a straight forward manner without any need to restrictive assumptions such as discretization or perturbation [13]. Because of saving space, the background of ADM is not presented herein. In order to acquaint ADM, the audiences are referred to Author's paper [9] and [13,24].

Herein, the general governing Eqs. (19), for a thermoelastic rotating disk with variable thickness and material properties subjected to lateral pressure is to be solved by ADM. In order to solve Eqs. (19),

the linear operators  $L_i$ ,  $i = 1, 2, 3$  corresponding to  $u_0(r)$ ,  $\varphi(r)$ ,  $w(r)$  can be respectively considered as:

$$\begin{aligned} L_1[u_0(r)] &= \frac{d^2 u_0(r)}{dr^2} \\ L_2[\varphi(r)] &= \frac{d^2 \varphi(r)}{dr^2} \\ L_3[w(r)] &= \frac{dw(r)}{dr} \end{aligned} \quad (29)$$

The initial approximations presented in Eqs. (21) are also considered in ADM.

Considering Eqs. (19) and ADM algorithm, one can suggest the nonlinear operators  $N_i$ ,  $i = 1, 2, 3$  corresponding with  $u_0(r)$ ,  $\varphi(r)$ ,  $w(r)$  respectively, as

$$\begin{aligned} N_1[u_0(r)] &= \frac{1}{rEh} \frac{d}{dr}(rEh) \frac{du_0}{dr} \\ &+ \frac{1}{rEh} \left( \nu \frac{d}{dr}(Eh) - \frac{Eh}{r} \right) u_0 - \frac{(1+\nu)}{Eh} \frac{d}{dr}(Eh\alpha T) \\ &+ \frac{(1-\nu^2)\rho r w^2}{E} \end{aligned} \quad (30a)$$

$$\begin{aligned} N_2[\varphi(r)] &= \frac{1}{rh^3 E} \left( h^3 r \frac{dE}{dr} + Eh^3 + 3h^2 \frac{dh}{dr} Er \right) \frac{d\varphi}{dr} \\ &- \frac{1}{r^2 h^3 E} \left( -h^3 r \nu \frac{dE}{dr} - 3h^2 \frac{dh}{dr} Er \nu + Eh^3 \right) \varphi \\ &+ \frac{12}{rEh^3} \left( \int r q_z dr - c_1 \right) (1-\nu^2) \end{aligned} \quad (30b)$$

$$\begin{aligned} N_3[w(r)] &= \varphi + \frac{2}{rEKh} (1+\nu) \left( \int r q_z dr \right) \\ &- \frac{2c_1}{rEKh} (1+\nu) \end{aligned} \quad (30c)$$

Now, Adomian's polynomials  $Y_{i,m}$  ( $m \geq 0$ ),  $i = 1, 2, 3$  for  $u_0(r)$ ,  $\varphi(r)$  and  $w(r)$  can be respectively determined as the following equations:

$$\begin{aligned} Y_{1,m}(u_{0,m}) &= \frac{1}{rEh} \frac{d}{dr}(rEh) \frac{du_{0,m}}{dr} \\ &+ \frac{1}{rEh} \left( \nu \frac{d}{dr}(Eh) - \frac{Eh}{r} \right) u_{0,m} \\ &+ \zeta_{m+1} \left[ -\frac{(1+\nu)}{Eh} \frac{d}{dr}(Eh\alpha T) + \frac{(1-\nu^2)\rho r w^2}{E} \right] \end{aligned} \quad (31a)$$

$$\begin{aligned} Y_{2,m}(\varphi_m) &= \frac{1}{rh^3 E} \left( h^3 r \frac{dE}{dr} + Eh^3 + 3h^2 \frac{dh}{dr} Er \right) \frac{d\varphi_m}{dr} \\ &- \frac{1}{r^2 h^3 E} \left( -h^3 r \nu \frac{dE}{dr} - 3h^2 \frac{dh}{dr} Er \nu + Eh^3 \right) \varphi_m \end{aligned}$$

$$+ \zeta_{m+1} \left[ \frac{12 \left( \int r q_z dr - c_1 \right) (1-\nu^2)}{rEh^3} \right] \quad (31b)$$

$$\begin{aligned} Y_{3,m}(w_m) &= \phi_m + \zeta_{m+1} \left[ \frac{2}{rEKh} (1+\nu) \left( \int r q_z dr \right) \right. \\ &\left. - \frac{2c_1}{rEKh} (1+\nu) \right] \end{aligned} \quad (31c)$$

In ADM, the higher terms of  $u_0(r)$  are determined by  $u_{0,m}(r) = -L^{-1}(N u_{0,m-1})$ ,  $m \geq 1$ . This manner can be followed to obtain the higher terms of  $\varphi(r)$  and  $w(r)$ . Hence, one has:

$$u_{0,m}(r) = - \int \int Y_{1,m-1}(u_{0,m-1}) dr dr + A_{1,m} + B_{1,m} r \quad (32a)$$

$$\varphi_m(r) = - \int \int Y_{2,m-1}(\varphi_{m-1}) dr dr + A_{2,m} + B_{2,m} r \quad (32b)$$

$$w_m(r) = - \int Y_{3,m-1}(\varphi_{m-1}) dr + A_{3,m} \quad (32c)$$

where  $A_{1,m}$ ,  $A_{2,m}$ ,  $A_{3,m}$  and  $B_{2,m}$  are integral constants which are determined by boundary conditions of Eq. (25). It is worth mentioning that  $c_1$  can also be determined by boundary condition of  $Q_r$  at outer radius of the disk.

By considering the disk model D (see Table 1), unknown functions  $u_{0,m}$ ,  $\varphi_m$  and  $w_m$  can be obtained by substituting Eqs. (31) into Eqs. (32). Therefore, the  $m$ th-order approximations of  $u_0$ ,  $\varphi$  and  $w$  can be expressed, respectively, as the Eqs. (27).

Herein, Eqs. (27) are the solution expressions. By imposing the boundary conditions (28) and using Eqs. (27) to  $u_0$ ,  $\varphi$  and  $w(r)$  and Eqs. (14a), (14c) and (14d) for  $N_r$ ,  $Q_r$  and  $M_r$ , respectively, one can easily determine the coefficients  $A_{1,0}$ ,  $A_{2,0}$ ,  $A_{3,0}$ ,  $B_{1,0}$ ,  $B_{2,0}$  and  $c_1$ .

### 3.3. Runge-Kutta's Method (RK)

To calculate Eqs. (19) by well-known Runge-Kutta's (RK) method, Eq. (19a), (19b) and (19c) must be solved in turn. In order to have numerical solution, the value of  $c_1$  of clamped-free boundary conditions must be firstly obtained by the following equation:

$$c_1 = \int r q_z(r) dr \quad \text{at} \quad r = b \quad (33)$$

For numerical solution, Eqs. (19a) and (19b) have to be rewritten in the form of:

$$\frac{d^2 \psi}{dr^2} = f \left( r, \psi, \frac{d\psi}{dr} \right) \quad (34)$$

in which  $\psi$  is a general unknown function. Here means  $u_0$  or  $\varphi$  which have the second order ordinary differential equations, i.e. Eqs. (19a) and (19b). In the RK method, the following equations are to be used [25]:

$$\left(\frac{d\psi}{dr}\right)_{i+1} = \left(\frac{d\psi}{dr}\right)_i + \frac{\Delta r}{6}(K_1 + 2k_2 + 2k_3 + k_4) \quad (35a)$$

$$\psi_{i+1} = \psi_i + \Delta r \left( \left(\frac{d\psi}{dr}\right)_i + \frac{\Delta r}{6}(k_1 + k_2 + k_3) \right) \quad (35b)$$

where  $\Delta r$  is step length in the radial direction of the disk. The  $k_i$  coefficients are calculated by

$$\begin{aligned} k_1 &= f\left(r_i, \psi_i, \left(\frac{d\psi}{dr}\right)_i\right) \\ k_2 &= f\left(r_i + \frac{\Delta r}{2}, \psi_i + \frac{\Delta r}{2} \left(\frac{d\psi}{dr}\right)_i, \left(\frac{d\psi}{dr}\right)_i + \frac{\Delta r}{2} k_1\right) \\ k_3 &= f\left(r_i + \frac{\Delta r}{2}, \psi_i + \frac{\Delta r}{2} \left(\frac{d\psi}{dr}\right)_i + \frac{1}{4} \Delta r^2 k_1, \left(\frac{d\psi}{dr}\right)_i + \frac{\Delta r}{2} k_2\right) \\ k_4 &= f\left(r_i + \Delta r, \psi_i + \Delta r \left(\frac{d\psi}{dr}\right)_i + \frac{1}{2} \Delta r^2 k_2, \left(\frac{d\psi}{dr}\right)_i + \Delta r k_3\right) \end{aligned} \quad (36)$$

Eq. (19c) is a first-order differential equation which its solution by RK method needs to be proceeded by the following algorithm.

Eq. (19c) has to be firstly rewritten as the following equation:

$$\frac{dw}{dr} = g(r, w, \varphi) \quad (37)$$

For the first order differential equation, following equation is to be used [25]:

$$w_{i+1} = w_i + \frac{1}{6}(k_1 + 2k_2 + 2k_3 + k_4) \quad (38)$$

where the  $k_i$  coefficients are calculated from

$$\begin{aligned} k_1 &= \Delta r g(r_i, w_i, \varphi_i) \\ k_2 &= \Delta r g\left(r_i + \frac{\Delta r}{2}, w_i + \frac{1}{2} k_1, \varphi_i\right) \\ k_3 &= \Delta r g\left(r_i + \frac{\Delta r}{2}, w_i + \frac{1}{2} k_2, \varphi_i\right) \\ k_4 &= \Delta r g(r_i + \Delta r, w_i + k_3, \varphi_i) \end{aligned} \quad (39)$$

It is worth mentioning that execution of the numerical solution starts from the inner boundary with a trial

value of the first-order derivative of the unknown functions ( $u_0$  and  $\varphi$ ). The procedure proceeds in an iterative and incremental manner. Here, the unknown functions can be determined by the boundary conditions on the outer radius of the disk.  $M_r$  and (for  $u_0$  and  $\varphi$ , respectively) must be equal to zero at outer radius of the disk. In the next increment in the radial direction with the step length  $\Delta r$ , the unknown functions and its first-order derivative at the new radius can be obtained using Eqs. (35). The unknown function  $w$ , with initial value  $w = 0$  may be easily obtained by Eq. (38).

### 3.4. Finite Element Method (FE)

A finite element analysis of rotating disk with non-uniform thickness and material properties is performed using the commercial available software [26]. The element SHELL181 was used to analyze the problem. It is worthy to be said that SHELL181 is suitable for analyzing thin to moderately-thick shell structures. It is a four-node element with six degrees of freedom at each node: translations in the x, y, and z directions, and rotations about the x, y, and z-axes. SHELL181 is well-suited for linear, large rotation and large strain nonlinear applications. The accuracy in modeling is governed by the Mindlin's first-order shear deformation theory [26].

It is noted that in the present study, the element SHELL181 was used in the elastic zone to analyze the bending of thin and moderately-thick rotating disks. Fig. 3 shows the modeled rotating disk and imposing associated loading and boundary conditions. As seen in Fig. 3, in order to decrease CPU-time, the one-fourth disk was modeled and then the associated boundary conditions were imposed as will be next explained.

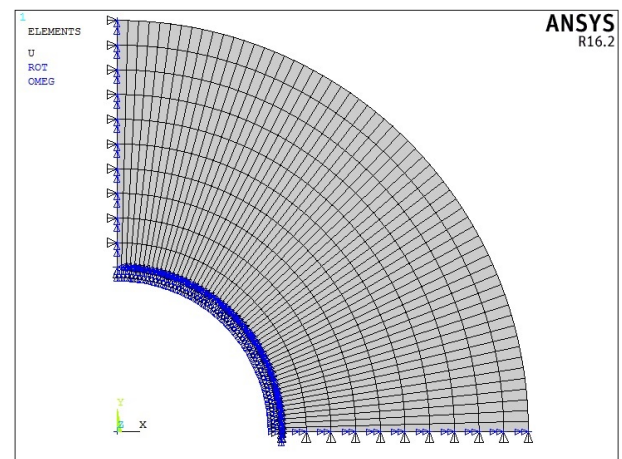


**Fig. 3.** Finite element model, meshing and imposing boundary conditions (Real meshing is so much finer).

In order to impose loading and boundary conditions, the disk rotates about central axis at constant angular velocity, in addition, for the sake of one-fourth-

modeled rotating disk, the symmetric boundary conditions in two edges of the model at degree of zero and  $\pi/2$  radians were imposed. The inner radius of the disk was clamped by constraining all degree of freedoms, i.e. UX, UY, UZ, ROTX, ROTY and ROTZ. The outer radius of the disk, which is free of any traction, was held unchanged. In order to achieve the adequate accuracy, the disk was discretized into 100 segments in radial direction. In each segment, the thickness and properties of disk were assumed constant and corresponding to their values at given radius defined by Eqs. (1) and (2).

### 4. Results and Discussion

In this section, results from HAM and ADM are presented and compared with those obtained by Runge-Kutta's and finite element solution. Fig. 4 to Fig. 6 show the distribution of functions  $u_0(r)$ ,  $\varphi(r)$  and  $w(r)$  against disk radius resulted by HAM, ADM, RK, and FEM for disk model D respectively.

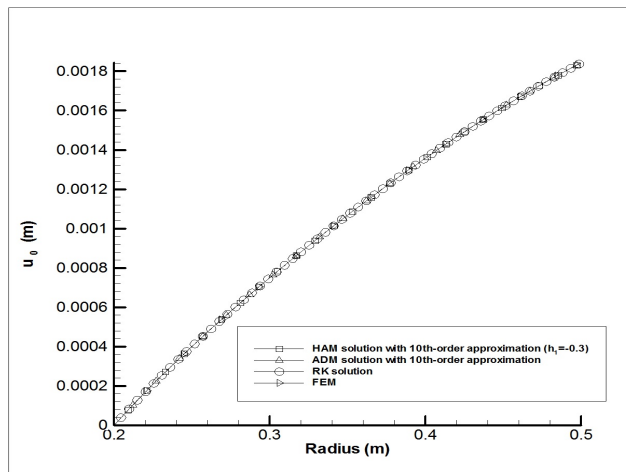


**Fig. 4.** The distribution of function  $u_0(r)$  obtained by HAM, ADM, RK and FEM for model D.

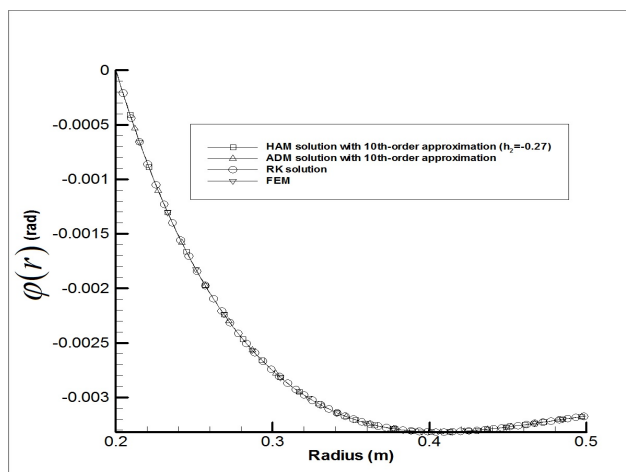


**Fig. 5.** The distribution of function  $\varphi(r)$  obtained by HAM, ADM, RK and FEM for model D.

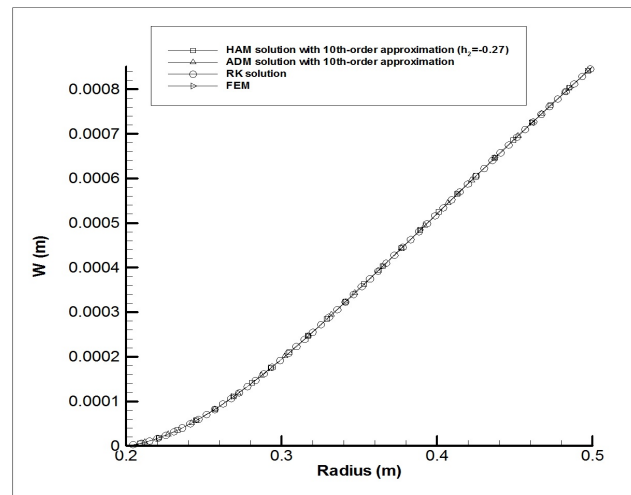


**Fig. 6.** The distribution of function  $w(r)$  obtained by HAM, ADM, RK and FEM for model D.

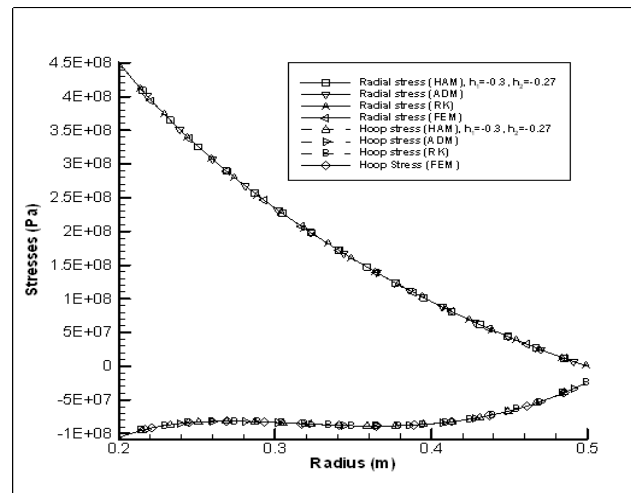


**Fig. 7.** Comparison of calculated stresses by HAM, ADM, RK and FEM of model D at  $z = -h(r)/2$ .

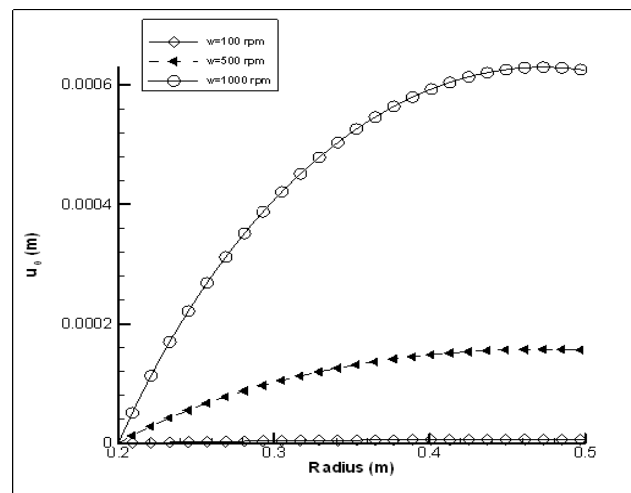


**Fig. 8.** The distribution of  $u_0(r)$  versus the radius of the disk with respect to the angular velocity.

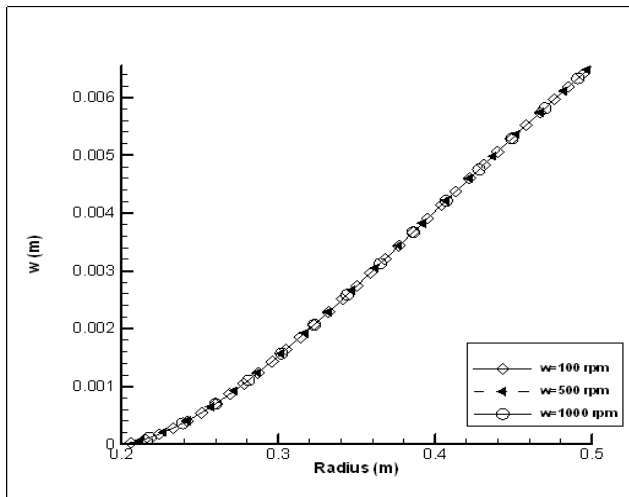


**Fig. 9.** The distribution of  $w(r)$  versus the radius of the disk with respect to the angular velocity.

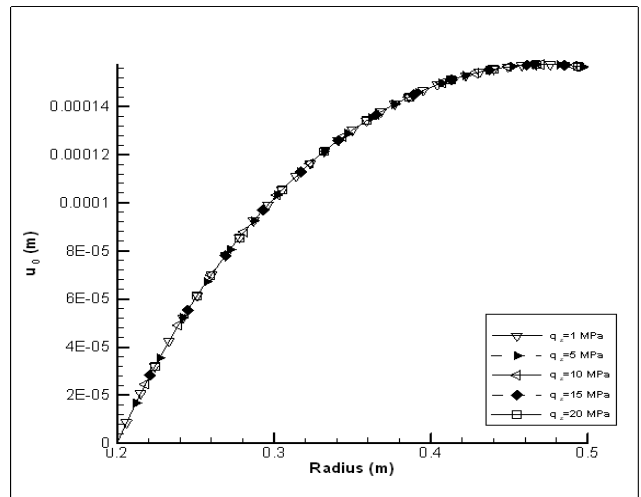


**Fig. 12.** The distribution of  $u_0(r)$  versus the radius of the disk with respect to the lateral pressure.

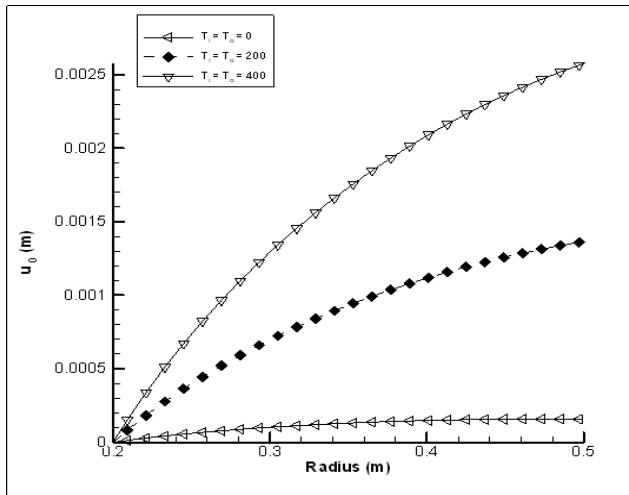


**Fig. 10.** The distribution of  $u_0(r)$  versus the radius of the disk with respect to the temperature gradient.

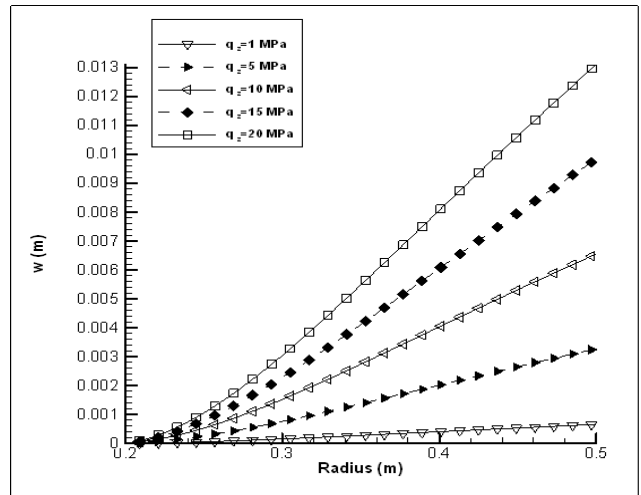


**Fig. 13.** The distribution of  $w(r)$  versus the radius of the disk with respect to the lateral pressure.

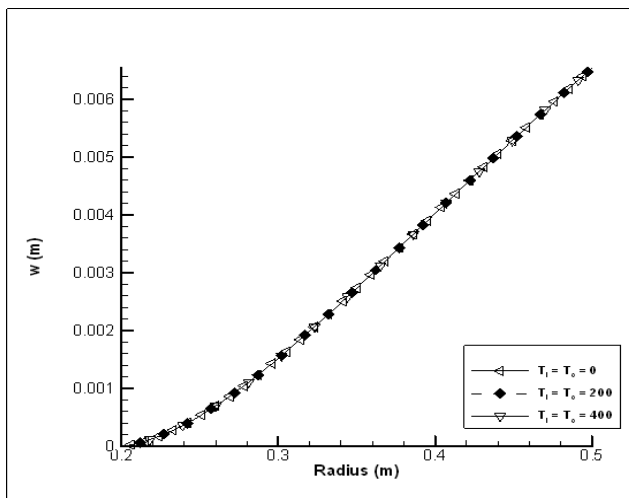


**Fig. 11.** The distribution of  $w(r)$  versus the radius of the disk with respect to the temperature gradient.

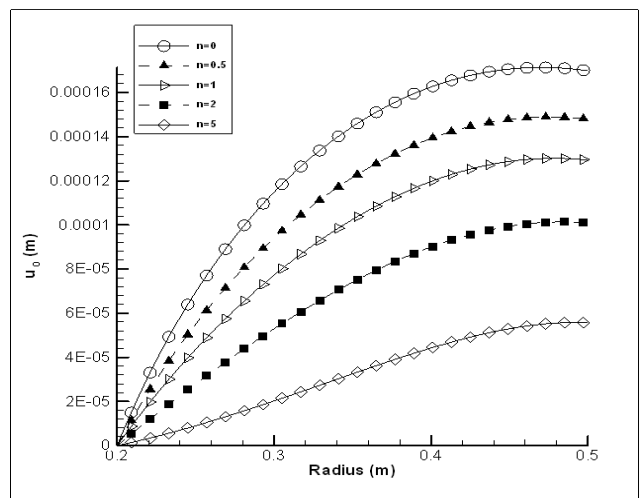


**Fig. 14.** The distribution of  $u_0(r)$  versus the radius of the disk with respect to the grading index.

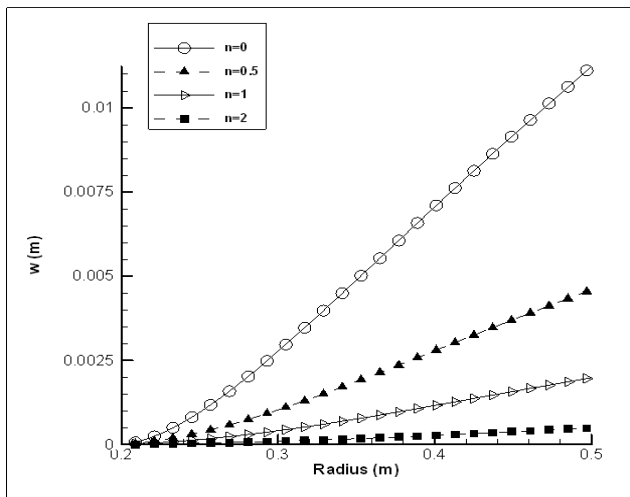


**Fig. 15.** The distribution of  $w(r)$  versus the radius of the disk with respect to the grading index.

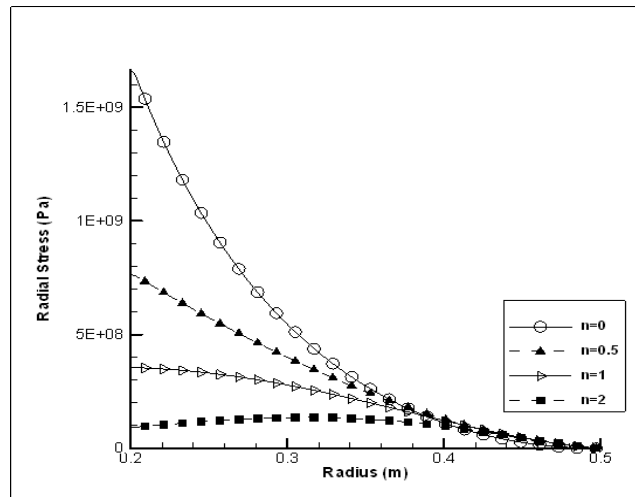


**Fig. 18.** The radial stress versus the radius of the disk with respect to the grading index.

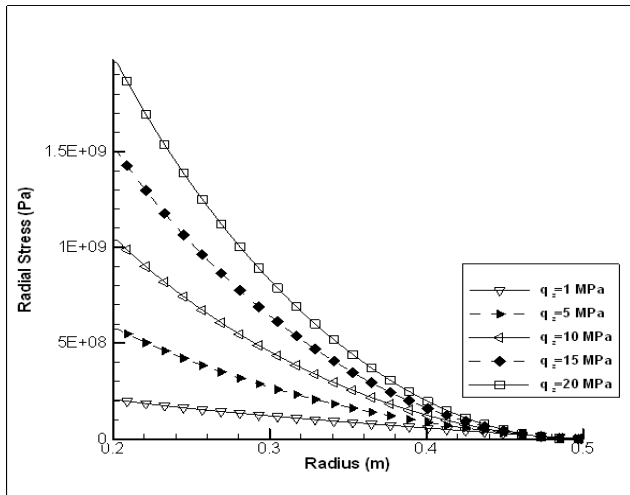


**Fig. 16.** The radial stress versus the radius of the disk with respect to the lateral pressure.

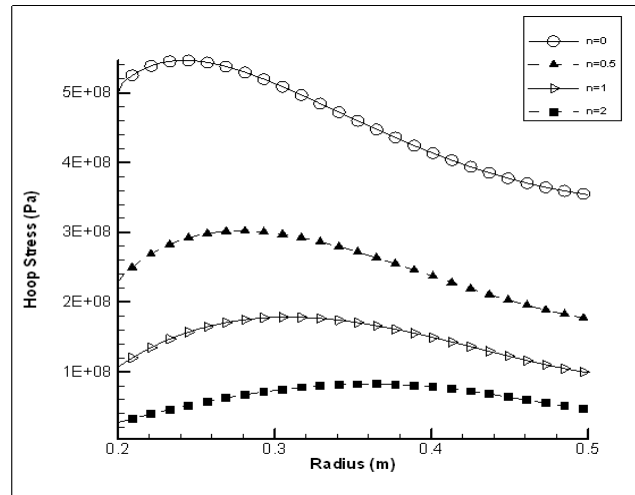


**Fig. 19.** The hoop stress versus the radius of the disk with respect to the grading index.

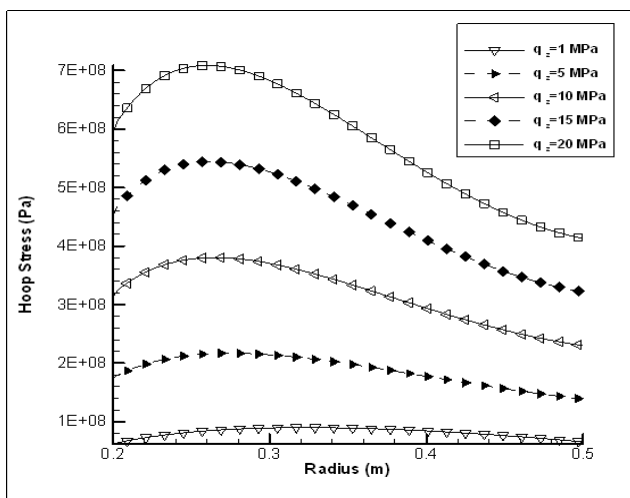


**Fig. 17.** The hoop stress versus the radius of the disk with respect to the lateral pressure.

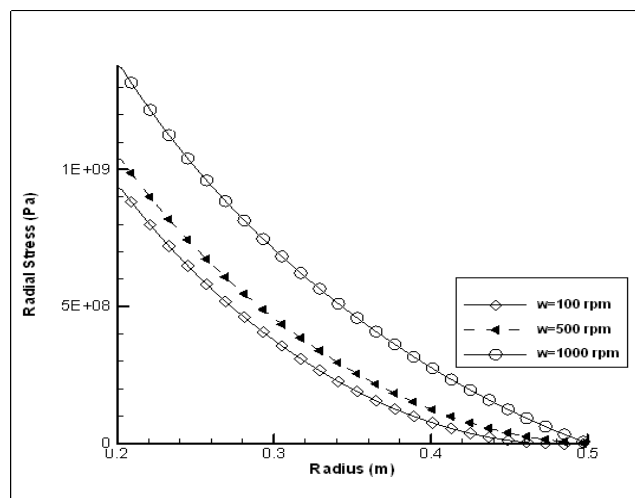


**Fig. 20.** The hoop stress versus the radius of the disk with respect to the angular velocity.

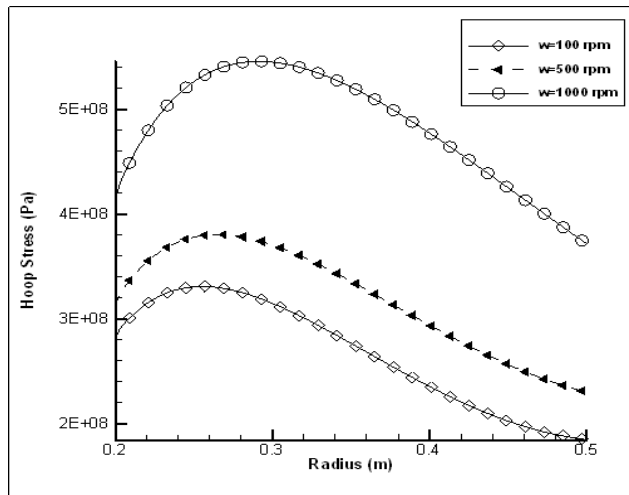


**Fig. 21.** The hoop stress versus the radius of the disk with respect to the angular velocity.

By using the solution of  $u_0(r)$ ,  $\varphi(r)$  and applying Eqs. (5), one can easily obtain the distributions of components of stress. Fig. 7 presents the radial and hoop stresses of disk model D at  $z = -h(r)/2$ , calculated by HAM, ADM, RK and FE methods. Fig. 4 to Fig. 7 obviously display that the results of four methods are in excellent agreements. Therefore, it induces that practiced methods have excellent ability of solving the moderately thick functionally graded thermoelastic rotating disks subjected to bending loading based on the Mindlin's theory.

In model D at  $z = -h(r)/2$ , the maximum stress component is the radial stress occurring at inner radius of the disk. The radial stress continuously reduces from the maximum point at inner radius to minimum position at outer radius. By considering Fig. 7, it is obvious that the hoop stress has its minimum value at inner radius, while; its maximum value occurs at outer radius of the disk. The hoop stress increases from inner radius up to a position within the disk, then decreases from that position up to another position within the disk, and then again increases from the latter position up to its maximum value at outer radius. It is worthwhile that the variations of hoop stress of model D against those of radial stress are trivial. In addition, it is necessary to notice that if there is no thermal loading, the angular velocity leads to positive radial and hoop stresses throughout the disk. Whereas, the thermal loading alone causes the negative hoop stress throughout the disk. As seen in Fig. 7, the circumferential stress is negative throughout the disk due to imposing both the angular velocity and thermal loading, simultaneously. It means that in the special model of the disk and loading (model D), presented in Table (1), the influence of thermal loading is greater than that of angular velocity to distribute the hoop stress of the rotating disk.

As final words, it can be said that the implemen-

tation of the proposed methods demonstrates the applicability of the HAM and ADM to provide accurate enough solution for a complicated case with no exact solution.

Fig. 8 and Fig. 9 show the variations of  $u_0$  and  $w$  with the changes of the angular velocity  $w$  of the model D, respectively. Fig. 8 and Fig. 9 demonstrate that the radial displacement of the middle surface of the disk  $u_0(r)$  increases with the increase in angular velocity, whereas angular velocity plays no role in determination of deflection  $w$ . This implies the fact that the differential equations of  $u_0(r)$  and  $w(r)$  are uncoupled due to linearity. In the other words, the unknown functions  $u_0(r)$  and  $w(r)$  are coupled if the governing differential equations are non-linear. Fig. 10 and Fig. 11 show the influence of temperature on the radial displacement,  $u_0$ , and deflection,  $w$ , respectively. As seen in Fig. 10, the increase in temperature gives rise to increase in radial displacement of mid-plane  $u_0$ , while the variations of temperature has no influence on the deflection. This fact can be easily derived through differential equations (15b) and (15c). The terms  $\alpha T$  doesn't exist in the equations related to  $w$  and  $\phi$ . In the view of physical interpretation, when there are no temperature gradients in thickness direction, it is not expected any deflection. Fig. 12 and Fig. 13 display the variations of radial displacement  $u_0$  and deflection  $w$  against lateral pressure  $q_z$ . As revealed in Fig. 12, the lateral loading  $q_z$  plays no role in radial displacement of the middle surface of the disk. This is fully comprehended due to the concepts of Mindlin's theory of plates. It is that the middle surface of the plate has no stretch due to bending loading. As it can be seen in Fig. 13, the increase in lateral pressure  $q_z$  causes increase in deflection  $w$ . Fig. 14 and Fig. 15 show the role of grading index on the radial displacement,  $u_0$ , and the deflection,  $w$ . As seen, the increase in grading index gives rise to decrease in both  $u_0$  and  $w$ . Fig. 16 and Fig. 17 display the influence of lateral pressure  $q_z$  on the radial and circumferential stresses, respectively. As expected, the growth of lateral pressure leads to increase in both components of stress. Fig. 18 and Fig. 19 present the effect of grading index on the radial and circumferential stresses respectively. As it can be seen, the increase in grading index results in decrease in radial and hoop stresses. It can be resulted from Fig. 14 and Fig. 15 related to the influence of grading index on  $u_0$  and  $w$ . It is obvious that the increase in both  $u_0$  and  $w$  are generally resulted in growth of both radial and hoop stresses. Fig. 20 and Fig. 21 show the role of angular velocity on the radial and hoop stresses respectively. As it can be expected, the increase in angular velocity leads to increase in both radial and hoop stresses.

It is worth mentioning that in order to clearly reveal the effects of various parameters with the exception of temperature on radial displacement  $u_0$ , deflection  $w$ ,

radial and hoop stresses, the temperature and its effects are vanished. In the other words, the temperature is only considered to derive Fig. 1 to Fig. 7 and Fig. 10 and Fig. 11.

## 5. Conclusions

In this paper, firstly, the governing differential equations of FGM rotating disk with variable thickness subjected to thermo-elastic and bending loadings through Mindlin's first order shear deformation theory were extracted. Then, two methods, namely Liao's homotopy analysis method (HAM) and Adomian's decomposition method (ADM) were applied to analyze the moderately-thick rotating disk. Such a study is undeniably required to realize how to treat some components such as brake disk and clutch. Comparing the results obtained by two methods with those of Runge-Kutta's and finite element methods (FEM), the correctness and reliability of the proposed methods for analysis of rotating disk were proven. With the help of results obtained by four methods, the components of stress were easily obtained by using calculated  $u_0(r)$ ,  $\varphi(r)$  and  $w(r)$  in HAM, ADM, RK and FEM. The curves and its variations of radial and hoop stresses of rotating disk were surveyed. For further investigation, the effects of angular velocity, lateral pressure, temperature and grading index on the radial displacement of mid-plane of the disk, deflection and on the radial and hoop stresses were demonstrated and discussed in detail.

## References

- [1] M. Bayat, B.B. Sahari, M. Saleem, A. Ali, S.V. Wong, Bending analysis of a functionally graded rotating disk based on the first order shear deformation theory, *Appl. Math. Model.*, 33 (2009) 4215-4230.
- [2] A.N. Eraslan, Y. Orcan, Elasticplastic deformation of a rotating solid disk of exponentially varying thickness. *Mech. Mater.*, 34 (2002) 423-32.
- [3] S.A.H. Kordkheili, R. Naghdabadi, Thermoelastic analysis of a functionally graded rotating disk, *Compos. Struct.*, 79 (2006) 508-16.
- [4] M. Bayat, M. Saleem, B.B. Sahari, A.M.S. Hamouda, E. Mahdi, Mechanical and thermal stresses in a functionally graded rotating disk with variable thickness due to radially symmetry loads, *Int. J. Pres. Ves. Pip.*, 86 (2009) 357-372.
- [5] M.H. Hojjati, S. Jafari, Variational iteration solution of elastic non uniform thickness and density rotating disks, *Far. East. J. Appl. Math.*, 29 (2007) 185-200.
- [6] M.H. Hojjati, S. Jafari, Semi-exact solution of elastic non-uniform thickness and density rotating disks by homotopy perturbation and Adomian's decomposition methods. Part I: Elastic solution, *Int. J. Pres. Ves. Pip.*, 85 (2008) 871-879.
- [7] M.H. Hojjati, S. Jafari, Semi-exact solution of non-uniform thickness and density rotating disks. Part II: Elastic strain hardening solution, *Int. J. Pres. Ves. Pip.*, 86 (2009) 307-18.
- [8] M.H. Hojjati, A. Hassani, Theoretical and numerical analyses of rotating discs of non-uniform thickness and density, *Int. J. Pres. Ves. Pip.*, 25 (2008) 695-700.
- [9] A. Hassani, M.H. Hojjati, G. Farrahi, R.A. Alashti, Semi-exact elastic solutions for thermo-mechanical analysis of functionally graded rotating disks, *Compos. Struct.*, 93 (2011) 3239-3251.
- [10] A. Hassani, M.H. Hojjati, G. Farrahi, R.A. Alashti, Semi-exact solution for thermo-mechanical analysis of functionally graded elastic-strain hardening rotating disks, *Commun. Nonlinear. Sci. Num. Simulat.*, 17 (2012) 3747-3762.
- [11] A. Hassani, M.H. Hojjati, E. Mahdavi, R.A. Alashti, G. Farrahi, Thermo-mechanical analysis of rotating disks with non-uniform thickness and material properties, *Int. J. Pres. Ves. Pip.*, 98 (2012) 95-101.
- [12] A. Hassani, M.H. Hojjati, A.R. Fathi, In-Plane free vibrations of annular elliptic and circular elastic plates of non-uniform thickness under classical boundary conditions, *Int. Rev. Mech. Eng.*, 4 (2010) 112-119.
- [13] G. Adomian, Solving frontier problems of physics: the decomposition method. Boston: Kluwer Academic; 1994.
- [14] S.J. Liao, Beyond perturbation: introduction to the homotopy analysis method. Boca Raton: Chapman and Hall/CRC Press; 2003.
- [15] S.A. Hosseini Kordkheili, M. Livani, Thermoelastic creep analysis of a functionally graded various thickness rotating disk with temperature-dependent material properties, *Int. J. Pres. Ves. Pip.*, (2013) 63-74.
- [16] M. Bayat, M. Rahimi, M. Saleem, A.H. Mohazab, I. Wudtke, H. Talebi, One-dimensional analysis for magneto-thermo-mechanical response in a functionally graded annular variable-thickness rotating disk, *Appl. Math. Model.*, 38 (2014) 4625-4639.

- [17] D. Ting, D. Hong-Liang, Thermo-elastic analysis of a functionally graded rotating hollow circular disk with variable thickness and angular speed, *Appl. Math. Model.*, 40 (2016) 7689-7707.
- [18] Hong-Liang Dai, Zhen-Qiu Zheng, Ting Dai, Investigation on a rotating FGPM circular disk under a coupled hygrothermal field, *Appl. Math. Model.*, 46 (2017) 28-47.
- [19] D. Ting, D. Hong-Liang, An analysis of a rotating (FGMEE) circular disk with variable thickness under thermal environment, *Appl. Math. Model.*, 45 (2017) 900-924.
- [20] R. Szilard, *Theories and applications of plate analysis: Classical, Numerical and Engineering Methods*, John Wiley & Sons, Inc; 2004.
- [21] S. Chakraverty, *Vibration of plates*, New York: CRC Press; Taylor & Francis group; 2009.
- [22] S.S. Rao, *Vibration of continuous systems*, John Wiley & Sons, Inc; 2007.
- [23] J.N. Reddy, C.M. Wang, S. Kitipornchai, Axisymmetric bending of functionally graded circular and annular plate, *Eur. J. Mech. A/Solids* 18 (1999) 185-199.
- [24] A.M. Wazwaz, *Partial differential equations and solitary waves theory*, Higher education Press, 2009.
- [25] C.F. Gerald, P.O. Wheatley. *Applied numerical analysis*. 6th ed. California: Addison-Wesley; 2002.
- [26] *User's Manual of ANSYS 16.2*, ANSYS Inc.; 2015.